International Journal of Nanomedicine

Dovepress
open access to scientific and medical research

Open Access Full Text Article

ORIGINAL RESEARCH

Immunogenic Cell Death Induced by Chemoradiotherapy of Novel pH-Sensitive Cargo-Loaded Polymersomes in Glioblastoma

Chen He[1]
Huiyan Ding[1]
Jing Chen[1]
Yinan Ding[1]
Rui Yang[2]
Chunmei Hu[3]
Yanli An[1]
Dongfang Liu[1]
Peidang Liu[1]
Qiusha Tang[1]
Zhiyuan Zhang[4]

[1]Medical School of Southeast University, Nanjing, People's Republic of China; [2]Research Institute for Reproductive Health and Genetic Diseases, The Affiliated Wuxi Maternity and Child Health Care Hospital of Nanjing Medical University, Wuxi, People's Republic of China; [3]Department of Tuberculosis, The Second Affiliated Hospital of Southeast University (The Second Hospital of Nanjing), Nanjing, People's Republic of China; [4]Department of Neurosurgery, Nanjing Jinling Hospital, Nanjing University, Nanjing, People's Republic of China

Background: Inducing the immunogenic cell death of tumour cells can mediate the occurrence of antitumour immune responses and make the therapeutic effect more significant. Therefore, the development of treatments that can induce ICD to destroy tumour cells most effectively is promising. Previously, a new type of pH-sensitive polymersome was designed for the treatment of glioblastoma which represents a promising nanoplatform for future translational research in glioblastoma therapy. In this study, the aim of this work was to analyse whether chemoradiotherapy of the novel pH-sensitive cargo-loaded polymersomes can induce ICD.

Methods: Cell death in U87-MG and G422 cells was induced by Au-DOX@PO-ANG, and cell death was analysed by CCK-8 and flow cytometry. The release of CRT was determined by using laser scanning confocal microscopy and flow cytometry. ELISA kits were used to detect the release of HMGB1 and ATP. The dying cancer cells treated with different treatments were cocultured with bone-marrow-derived dendritic cells (BMDCs), and then flow cytometry was used to determine the maturation rate of BMDCs (CD11c+CD86+CD80+) to analyse the in vitro immunogenicity. Tumour vaccination experiments were used to evaluate the ability of Au-DOX@PO-ANG to induce ICD in vivo.

Results: We determined the optimal treatment strategy to evaluate the ability of chemotherapy combined with radiotherapy to induce ICD and dying cancer cells induced by Au-DOX@PO-ANG+RT could induce calreticulin eversion to the cell membrane, promote the release of HMGB1 and ATP, and induce the maturation of BMDCs. Using dying cancer cells induced by Au-DOX@PO-ANG+RT, we demonstrate the efficient vaccination potential of ICD in vivo.

Conclusion: These results identify Au-DOX@PO-ANG as a novel immunogenic cell death inducer in vitro and in vivo that could be effectively combined with RT in cancer therapy.

Keywords: immunogenic cell death, ICD, glioblastoma, radiotherapy, polymersomes, nanodrug delivery system

Introduction

Glioblastoma (GBM) is the most aggressive primary intracranial tumour and one of the most severe challenges facing oncology.[1,2] The current clinical treatment is mainly surgery supplemented by chemotherapy and radiotherapy and many treatment strategies have been developed for the treatment of GBM.[3–7] In recent years, significant progress has been made in antitumour immunotherapy research. Some emerging immunotherapy methods have made major breakthroughs in the treatment of various types of tumours, such as the application of immune checkpoint blocker anti-PD-1 antibodies, which can

Correspondence: Qiusha Tang
Medical School of Southeast University, 87 Dingjiaqiao Road, Nanjing, People's Republic of China
Email panyixi-tqs@163.com

Zhiyuan Zhang
Department of Neurosurgery, Nanjing Jinling Hospital, Nanjing University, Nanjing, People's Republic of China
Email zzy8896@163.com

Received: 10 August 2021
Accepted: 14 October 2021
Published: 22 October 2021

restore the killing effect of the immune system on tumour cells.[8] However, the low immunogenicity of glioblastoma cells and the existence of a tumour inhibitory immune microenvironment can hinder the application of these methods.[9] The induction of immunogenic cell death (ICD) may be a promising strategy. The concept of ICD suggests that some treatments can enhance the immunogenicity of tumour cells through multiple mechanisms when nonspecifically killing tumour cells and generate strong and long-lasting anticancer immunity by releasing tumour-associated antigens and damage-associated molecular patterns (DAMPs), such as exposure to calreticulin (CRT) at the cell surface and the release of HMGB1 and ATP.[10–14] The release of DAMPs promotes the maturation and migration of dendritic cells (DCs). Activated DCs can present tumour antigens to T cells and initiate T cell immune responses.[15,16]

Intracellular reactive oxygen species (ROS) might be one of the key factors for the induction of ICD, which could result in oxidative stress in organelles, including the endoplasmic reticulum.[17] Radiation therapy (RT) generates hydroxyl radicals (•OH) by using X-rays to damage tumour cellular components.[18] Consequently, RT could potentially induce ICD and prime the immune system.[19] However, the RT-mediated ICD effect is very weak, which may be due to insufficient ROS production. Tumour tissues would result in insufficient X-ray deposition and •OH generation because of low-Z elements.[20] According to recent studies, gold nanoparticles have been widely proven to be a radiosensitizer.[21–23] The absorption coefficient of gold nanoparticles for radiation is significantly higher than that of soft tissue, which can increase the absorbed dose of cells around the particles and the dose of X-ray deposition in the tumour area. The interaction of high atomic number gold atoms with kilovolt-level X-rays will produce secondary electronic levels and then promote the production of ROS.[24] Therefore, gold nanoparticles might have the ability to increase the RT-mediated ICD effect.

Moreover, previous studies have confirmed that chemotherapeutic drugs such as doxorubicin, oxaliplatin, mitoxantrone, and bortezomib can induce ICD. These chemotherapeutic drugs could promote the release of calreticulin (CRT), heat shock protein, high mobility group protein B1 (HMGB1), and ATP through endoplasmic reticulum (ER) stress while inducing the apoptosis of tumour cells.[25,26] However, the special anatomical structure of the brain prevents drugs from entering the brain. At the same time, chemotherapeutics have the shortcoming of a short half-life, which causes the weak ICD effect induced by chemotherapy drugs.[12,27,28] Many researchers are devoted to exploring new strategies to transform ICD into effective antitumour immunotherapy. Targeted nanocarriers are favoured because of their large drug loading, stable chemical properties, low or nontoxicity, biodegradability, and ability to target specific areas. The use of nanomaterials combined with chemotherapy drugs could solve the above problems.[29–31]

Previously, a new type of pH-sensitive polymersome was designed for the treatment of glioblastoma. (The polymersomes were formed through the self-assembly of polycaprolactone-poly(2-ethyl-2-oxazoline) (PCL-PEOz). A complex drug was synthesized from gold nanoparticles and doxorubicin. This type of complex drug could ensure that gold nanoparticles and doxorubicin were encapsulated into the vesicles in certain proportions at the same time. Modifying the Angiopep-2 peptide on the surface of polymersomes could solve the problem of poor delivery capacity through the BBB.) We have also proven that Angiopep-2-conjugated pH-sensitive polymersomes (Au-DOX@PO-ANG) can pass through the blood–brain barrier successfully and achieve a combination of radiotherapy and chemotherapy. The results have been published in the Journal of Nanobiotechnology.[32] Simultaneously, we found that the new type of nanodrug delivery system may have the ability to induce ICD in glioblastoma because of the existence of doxorubicin and gold nanoparticles. In this study, we investigated the ability of a new type of nanodrug delivery system to induce ICD. We demonstrate that glioblastoma U87-MG and G422 cells are induced to die by Au-DOX@PO-ANG combined with RT. These dying cancer cells can effectively induce the maturation of dendritic cells (Scheme 1). Using dying tumour cells after treatment with Au-DOX@PO-ANG combined with RT, the effective vaccination potential of ICD was demonstrated in a mouse glioblastoma vaccination model.

Experimental Section

Cell Culture

Human glioblastoma cell line U87-MG was purchased from National Collection of Authenticated Cell Cultures and murine glioma cell line G422 was purchased from Shanghai FuHeng Biology Co., Ltd. Human glioblastoma cell line U87-MG and murine glioma cell line G422 were cultured at 37 °C under 5% CO_2 in 1640 medium (containing 10% FBS and antibiotics).

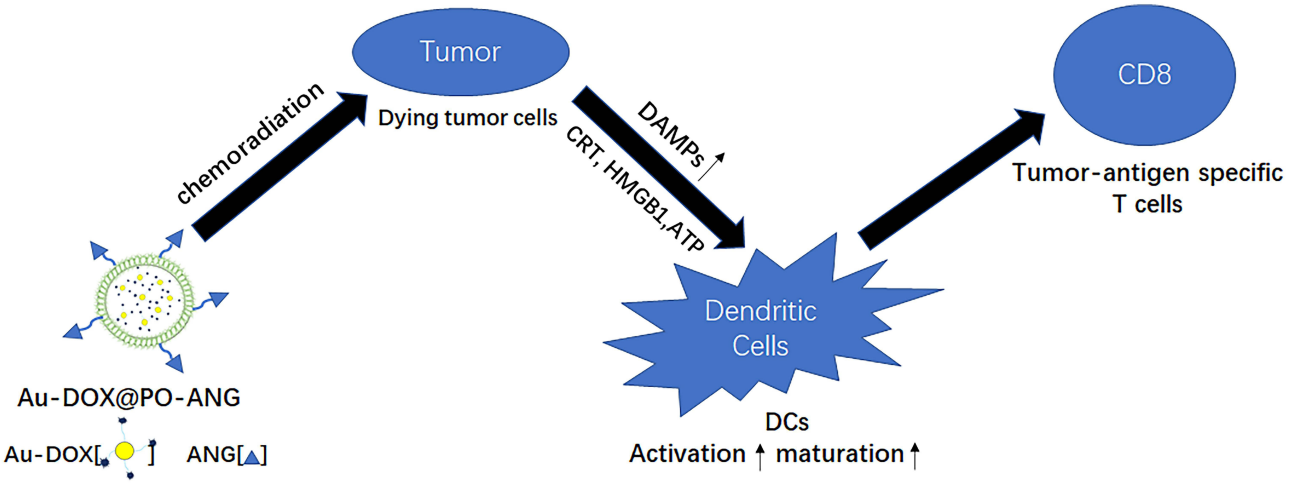

Scheme 1 Schematic illustration of ICD induced by chemoradiotherapy of novel pH-sensitive cargo-loaded polymersomes.

Preparation and Characterization of Au-DOX@PO-ANG

The methods of this part have been published in the Journal of Nanobiotechnology.[32]

The Detailed Groups in Subsequent Experiments

U87-MG and G422 cells were incubated with different groups. The detailed groups were as follows: 1) control, 2) blank polymersomes, 3) ANG-PO, 4) RT, 5) Au-DOX@PO-ANG, 6) Au-DOX@PO-ANG+RT. (The concentration of Au-DOX was 40 μg/mL in each group treated with G422 cells and 100 μg/mL in each group treated with U87-MG cells).

Cell Death Assay by Flow Cytometry and CCK8

The assay was performed by an ACEA NovoCyte flow cytometer, and FlowJo software was used to analyse the data. The CCK-8 assay was performed according to the instructions of the CCK-8 kit.

Analysis of CRT Exposure at the Cell Surface by Flow Cytometry

U87-MG and G422 cells were incubated with the "treatment" for 12 h in every group. Cells in every group were treated with radiotherapy after incubation at a dose of 6 Gy (according to previous reports, 6 Gy is a common dose for radiotherapy[33]) and then incubated at 37 °C under 5% CO_2 for 12 h. After incubation, the cells were collected and then washed with ice-cold PBS. After centrifugation at 1500 rpm and 4 °C for 5 min, the cells were resuspended in anti-calreticulin antibody in ice-cold PBS for 30 min at 4 °C and then washed with PBS three times. Finally, the samples were analysed by an ACEA NovoCyte flow cytometer. Analysis was performed by FlowJo software.

Immunofluorescence Analysis

U87-MG and G422 cells were seeded at a density of 1×10^5 cells per well in 6-well plates and then cultured for 24 h in a cell culture incubator. The cells were divided into six groups treated after attachment. The samples were washed three times with PBS and then incubated with Alexa Fluor 488-conjugated anti-CRT antibody for 30 min without light at 4 °C. After washing three times with ice-cold PBS, cells were fixed with 4% paraformaldehyde for 15 min and incubated with DiI at 37 °C for 10 min. Confocal fluorescence microscopy was used for immunofluorescence analysis (Nikon A1).

Evaluation of HMGB1 Release

Cells were incubated with the "treatment" for 12 h in every treatment group. Subsequently, cells were treated with radiotherapy at a dose of 6 Gy and then incubated for another 12 h. The supernatant of each group was collected and cleared from dying tumour cells by centrifugation at the indicated time points. HMGB1 quantification was measured by an ELISA kit. All assays were performed in accordance with the respective manufacturers' instructions.

Evaluation of ATP Release

U87-MG and G422 cells were stimulated with different groups as described above. Then, the supernatants were

collected and centrifuged at the indicated time points (15,000 rpm, 4 °C, 3 min). ATP analysis was performed using an ATP detection kit (Beyotime, S0026) as described by the manufacturer.

Extraction and Cultivation of Mouse Bone-Marrow-Derived Dendritic Cells

Bone-marrow-derived dendritic cells (BMDCs) were extracted from the femurs and tibias of C57BL/6J mice at the age of 6–7 weeks and cultured using 1640 medium (5% foetal calf serum, 20 ng/mL GM-CSF and 30 ng/mL IL-4 were contained). Fresh medium was added on Day 3, and the medium was renewed on Day 6 and Day 9.

Analysis of BMDCs Maturation

Immature murine BMDCs were isolated and cultured as described previously.[34] BMDCs were coincubated with dying U87-MG and G422 cells stimulated with different groups as described above. The cells were collected after coculture for 24 h, spun down at 400 g and 4 °C for 6 min, and then washed once with PBS. The maturation of BMDCs was analysed by flow cytometer immunostaining with anti-CD11c-FITC (Biolegend), anti-CD86-PE-Cy7 (Biolegend), and anti-CD80-APC (Thermo Fisher Scientific).

In vivo Prophylactic Tumour Vaccination

Dying G422 cells in different groups were collected and resuspended at the desired cell density in PBS. Mice were subcutaneously inoculated with 5×10^5 dying G422 cells into the left side. The mice were challenged subcutaneously in the right brain with 5×10^4 live G422 cells on Day 7 after vaccination. After the challenge, tumour growth at the challenge site was monitored using MRI imaging for up to 4 weeks. The levels of IFN-γ, TNF-α, and IL-12/p40 in mouse serum were measured by ELISA kits.

Statistical Analysis

The data were analysed using GraphPad Prism version 7.0 software (GraphPad Software, Inc., San Diego, CA, USA). Student's *t*-test was used when comparing the data from two groups. The differences between the two groups were considered statistically significant at $^*P < 0.05$ and very significant at $^{**}P < 0.01$ and $^{***}P < 0.001$.

Results

Preparation and Characterization of Au-DOX@PO-ANG

The results of this section have been published in the Journal of Nanobiotechnology.[32] The hydrodynamic diameter of the prepared Au-DOX was approximately 25.8 nm. The diameter was slightly larger than the modified AuNPs, but still less than 50 nm, which was conducive to encapsulation in polymersomes. TEM results revealed that the copolymer spontaneously assembled into polymersomes. The TEM images revealed a vesicle-like shape of blank polymersomes with average diameters of approximately 200 nm, consistent with the DLS results, and the Au-DOX complexes were located inside the polymersomes, suggesting that Au-DOX complexes were encapsulated in the polymersomes. Additionally, the amount of Au-DOX complexes in the polymersomes was clearly regulated by the amount of Au-DOX complexes added. The mean hydrodynamic diameter of blank polymersomes was 195.5 nm. After Au-DOX loading and ANG coupling, the mean hydrodynamic diameter increased slightly to 210.8 nm. The coupling efficiency was calculated by dividing the amount of Angiopep-2 on the surface of polymersomes by the weight of the Angiopep-2 input. After the calculation, the standard concentration curve formula for the ANG peptide was y=0.0044x-0.185 and the coupling efficiency was 11.3±1.02%. The particle number of polymersomes was measured using NTA and yielded a value of 6×10^{11} particles/mL. The number of ANG peptides connected to each polymersome was estimated to be 236. The drug loading capacity of Au-DOX in the polymersomes was approximately 5.3%, with an entrapment efficiency greater than 89.5% and an Au-DOX content of 0.725 mg/mL.

Au-DOX@PO-ANG Combined with RT Induces Cell Death in Cancer Cells

To evaluate the ability of chemotherapy combined with radiotherapy to induce ICD, the treatment strategy was adjusted in this study. Cells were incubated with the "treatment" for 12 h in every treatment group. Subsequently, cells were treated with radiotherapy at a dose of 6 Gy and then incubated for another 12 h. Cell Counting Kit-8 (CCK-8) was used to evaluate the antitumour capability of Au-DOX@PO-ANG in U87-MG cells. The results are shown in Figure 1A-1. Compared with the control group, the blank polymersomes and ANG-PO groups had no significant

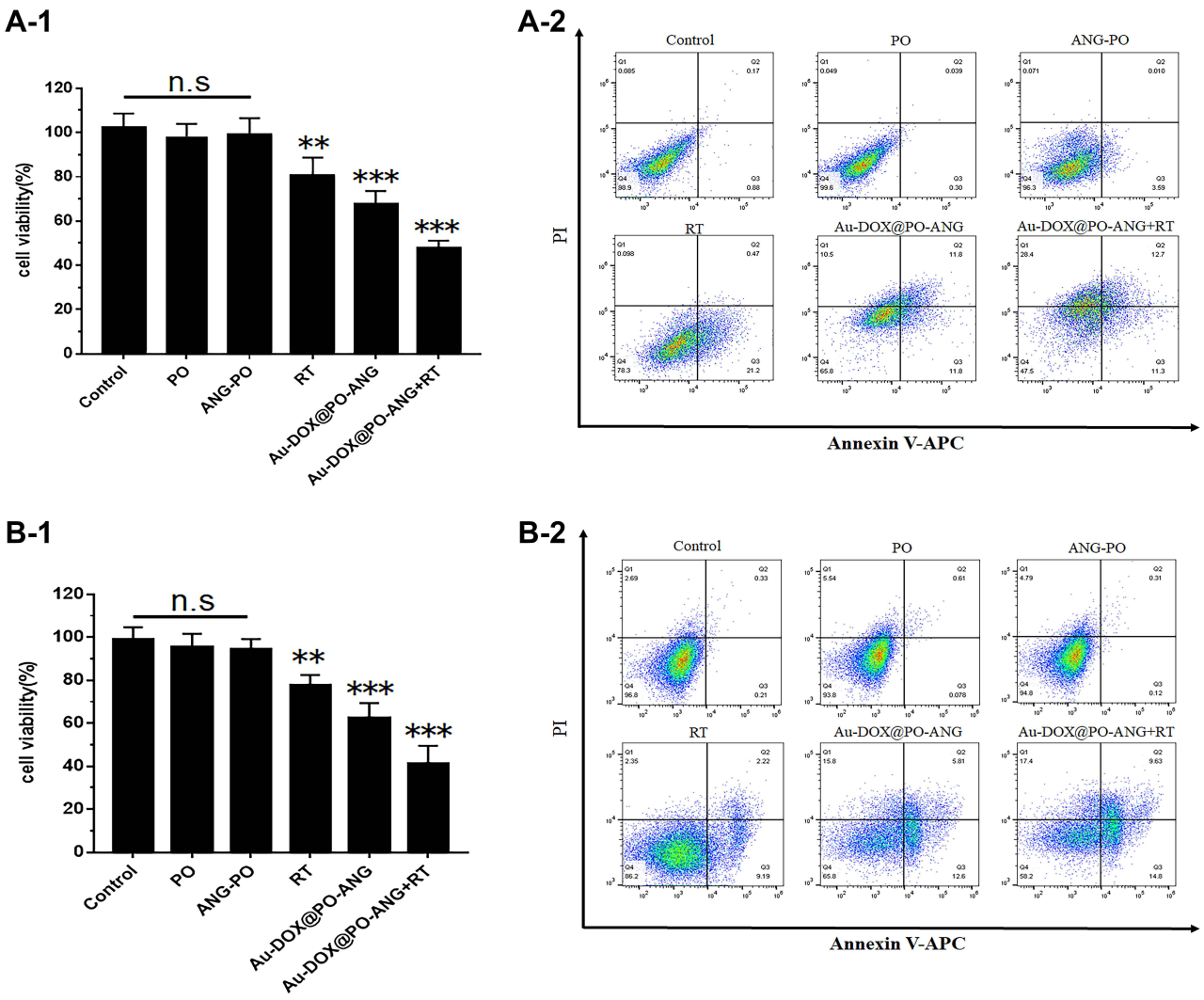

Figure 1 The antitumor capability of Au-DOX@PO-ANG combined with RT in vitro. Cell death assay by CCK8 (**A-1**) and flow cytometry (**A-2**) in U87-MG cells; cell death assay by CCK8 (**B-1**) and flow cytometry (**B-2**) in G422 cells. Each bar represents the mean± SD of six replicates, **P<0.01,***P<0.001.

effect on the cell survival rate of U87-MG cells. The survival rates of U87-MG cells treated with RT, Au-DOX@PO-ANG, and Au-DOX@PO-ANG+RT were 80.9± 8.2%, 67.5 ± 6.1% and 47.8 ± 3.3%, respectively. The results of the apoptosis experiment using an Annexin-V/PI staining kit (Figure 1A-2) show that Au-DOX-loaded polymersomes and radiotherapy can induce U87-MG cell apoptosis, and the viable cell ratio of the Au-DOX@PO-ANG+RT group was significantly lower than that of the Au-DOX@PO-ANG group and RT group. Similar results were obtained in G422 cells (Figure 1B). These results show that the Au-DOX@PO-ANG+RT group has stronger cytotoxicity than the other treatment groups. To evaluate the ICD effect, the drug concentration in the Au-DOX@PO-ANG+RT group will be controlled at approximately the IC50.

ICD Induction

The occurrence of ICD in tumour cells is accompanied by the release of damage-related molecular patterns (DAMPs), such as surface exposure to CRT and the release of HMGB1 and ATP. DAMPs have a beneficial role in anticancer therapy because of their interaction with the innate immune system.[15,16,35] During ICD, CRT acts as an “eat me” signal and can be translocated from the endoplasmic reticulum (ER) to the surface of dying cells. This signal can help to promote the absorption of dying tumour cells by antigen-presenting cells, activating T lymphocytes and leading to antigen-specific immune responses.[34] The ICD profile induced by different treatments was investigated by examining cell-surface CRT expression. We first employed immunostaining analysis by confocal fluorescence

microscopy. Cell surface delineation was determined using Dil (Dil was used for cell membrane localization) (red), and Alexa Fluor 488-CRT antibody was used for determination of CRT expression (green). As shown in Figures 2A and 3A, the two cell lines used in this study reached a similar conclusion. The CRT signals were found in the RT and Au-DOX@PO-ANG groups. However, the signal of the RT group was weak, indicating the inferior ability of X-rays to induce ICD. Furthermore, the strongest CRT signal was found from the Au-DOX@PO-ANG+RT

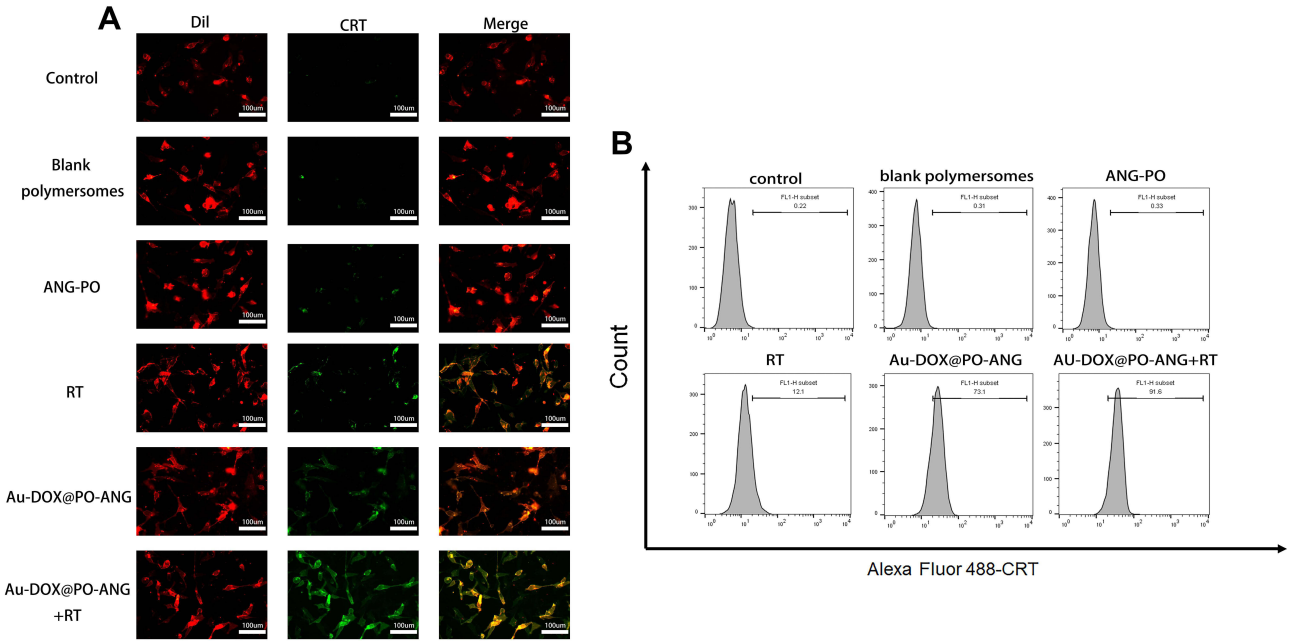

Figure 2 (**A**) Confocal microscopy showing the induction of the ICD marker, CRT, in U87-MG cells after different treatments. The cell surface membrane and CRT were detected by Dil, and Alexa Fluor 488-conjugated anti-CRT antibody staining (scale bar: 100 μm). (**B**) CRT exposure on the cell surface of U87-MG cells was assessed after the different treatments by flow cytometry analysis.

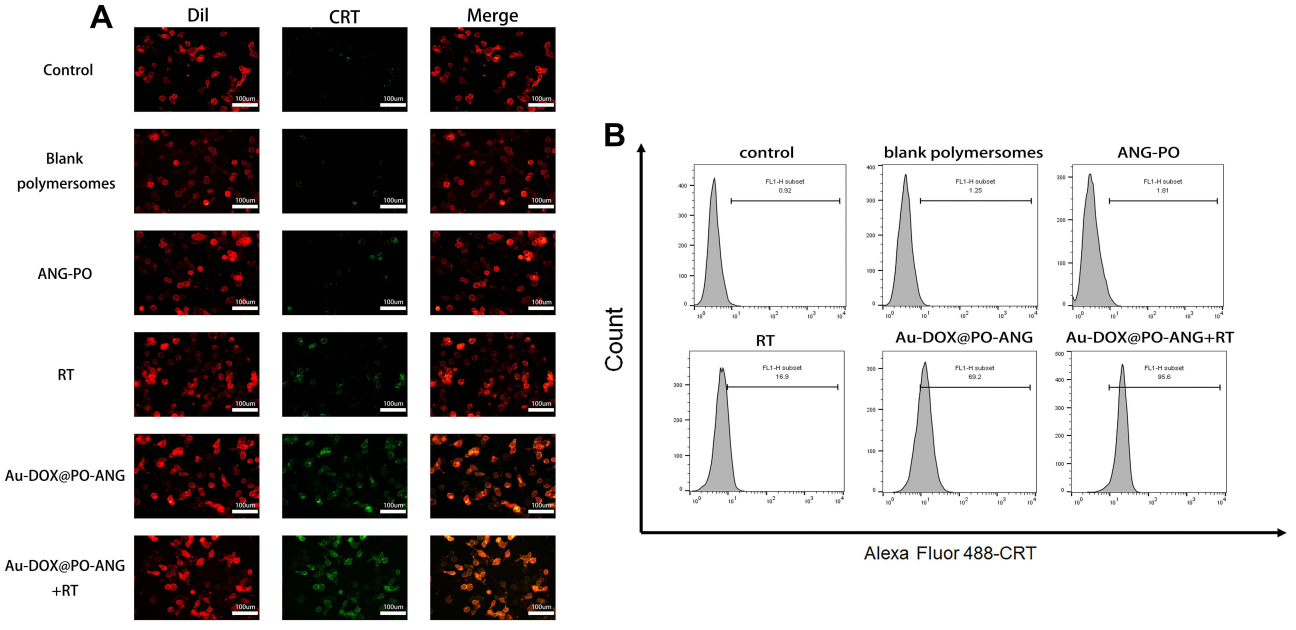

Figure 3 (**A**) Confocal microscopy showing the induction of the ICD marker, CRT, in G422 cells after different treatments. The cell surface membrane and CRT were detected by Dil, and Alexa Fluor 488-conjugated anti-CRT antibody staining (scale bar: 100 μm). (**B**) CRT exposure on the cell surface of G422 cells was assessed after the different treatments by flow cytometry analysis.

group, indicating that the most significant ICD could be induced by the combination of Au-DOX@PO-ANG and X-rays. In addition, no green fluorescence was detected in the group of blank polymersomes or Angiopep-2 conjugated polymersomes, implying no ICD induced by the nanocarriers or targeting peptides. Flow cytometry results further confirmed that Au-DOX@PO-ANG combined with X-ray radiation could significantly promote cell-surface expression of CRT in U87 and G422 cells, demonstrating the strongest ICD induced by Au-DOX@PO-ANG-mediated RT over other groups (Figures 2B and 3B). In summary, these results indicate that Au-DOX@PO-ANG combined with RT has promising potential to enhance tumour immunogenicity.

HMGB1 is a danger signal that can stimulate phagocytosis of dying tumour cells by DCs. HMGB1 is mainly located in the nucleus of cells.[34] Figure 4A and B shows that RT, Au-DOX@PO-ANG, and Au-DOX@PO-ANG combined with RT induced the release of HMGB1. In contrast, HMGB1 was released the most from the nucleus in the Au-DOX@PO-ANG combined RT group in both U87 and G422 cells. The average concentration of

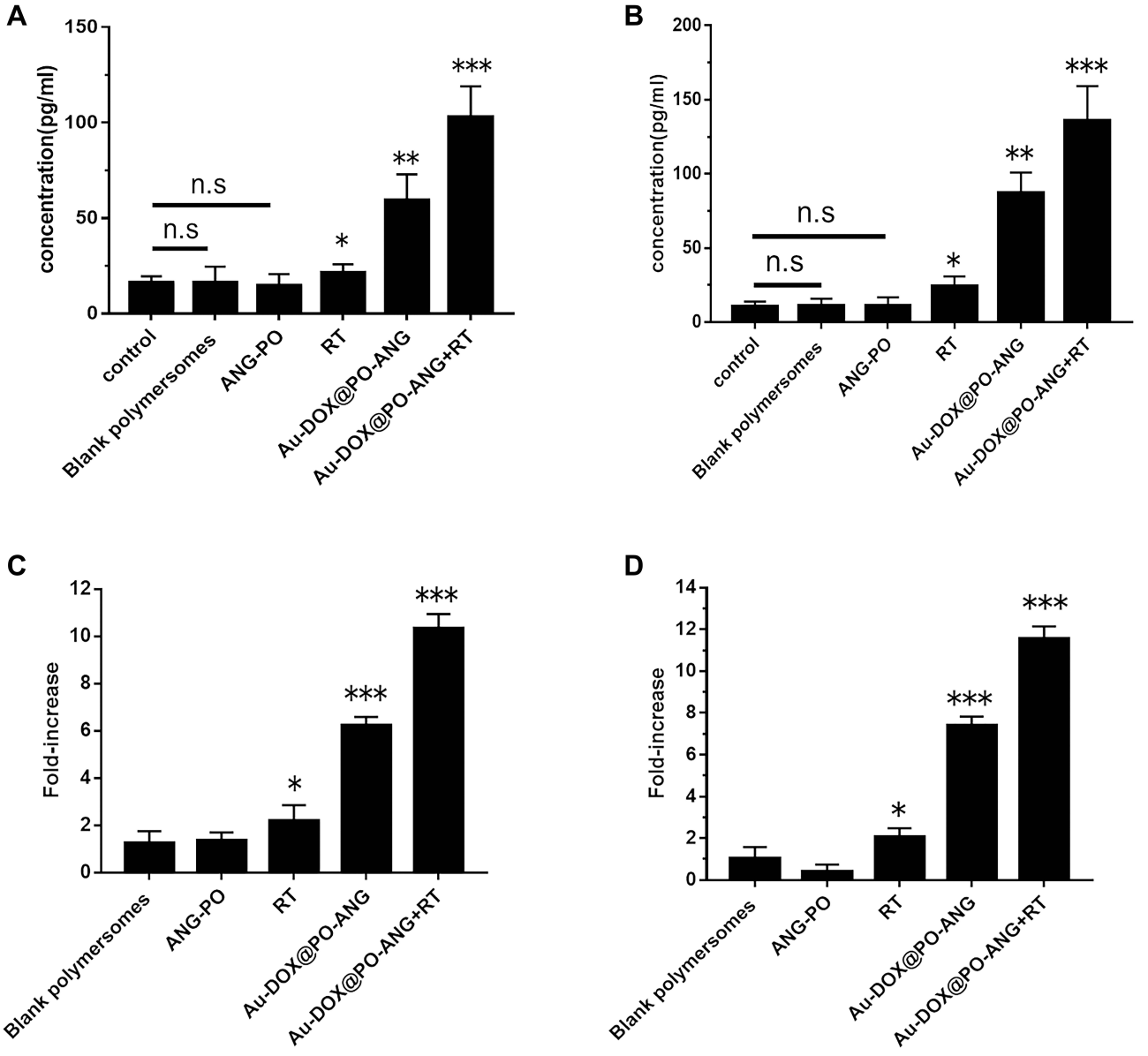

Figure 4 The release of HMGB1 and ATP. U87-MG (**A**) and G422 cells (**B**) were recovered for 24h after different treatments and HMGB1 was measured in the supernatants; U87-MG (**C**) and G422 cells (**D**) were recovered for 24h after different treatments and ATP was measured in the supernatants. ATP values represent fold increase relative to untreated cells and the mean values of 6 independent experiments. Each bar represents the mean± SD of six replicates, *P<0.05,**P<0.01,***P<0.001.

HMGB1 released from U87 cells of the Au-DOX@PO-ANG + RT group was 103.1 pg/mL, which was 4.8- and 1.7-fold higher than those of the RT and Au-DOX@PO-ANG groups, respectively (Figure 4A). The results were similar in G422 cells. The average concentration of HMGB1 released from G422 cells of the Au-DOX@PO-ANG + RT group was 135.9 pg/mL, which was 5.6- and 1.6-fold higher than those of the RT and Au-DOX@PO-ANG groups, respectively (Figure 4B).

Moreover, U87 cells treated with Au-DOX@PO-ANG + RT showed that the highest ATP secretion was 10.3-fold higher than that of the control group (Figure 4C). Similarly, the quantity of ATP secreted by the Au-DOX@PO-ANG + RT group in G422 was 11.5-fold higher than that of the control group (Figure 4D). In both types of cells, the release of HMGB1 and the secretion of ATP were not observed in the blank polymersomes or ANG-PO group. These results indicate that neither the carrier nor the targeting peptide used in this study has the ability to induce ICD.

Collectively, the CRT exposure, the release of HMGB1, and ATP secretion data verified that Au-DOX@PO-ANG-based chemotherapy and RT cumulatively induced ICD in vitro.

Activation and Maturation of BMDCs

Treatment-induced antitumour immunity was further investigated by examining BMDC maturation. BMDCs were freshly separated from C57BL/6J mice and incubated with U87-MG and G422 cells pretreated with different treatments. The frequency of mature BMDCs (CD11c + CD86 + CD80+) was then examined by flow cytometry. Figure 5A shows that after 24 hours of incubation with untreated U87-MG cells, the maturity of BMDCs was low due to the low immunogenicity of tumour cells. A low level of BMDC maturity was also observed in the blank polymersomes group and ANG-PO group due to the negligible lethality of the carrier and the targeting peptide. When BMDCs were incubated with RT- and Au-DOX@PO-ANG-pretreated U87-MG cells, the frequency of mature BMDCs moderately increased by 1.6- and 2.3-fold, respectively, compared to that of BMDCs incubated with untreated U87-MG cells. In addition, U87-MG cells pretreated with Au-DOX@PO-ANG + RT showed the strongest ability to induce BMDC maturation. The BMDC maturation rate was further promoted 2.9-fold. Similar results were observed in G422 cells (Figure 5B); the frequency of mature BMDCs moderately increased by 1.6-, 1.8-, and 2.0-fold when the BMDCs were incubated with RT-, Au-DOX@PO-ANG-, and Au-DOX@PO-ANG + RT-pretreated G422 cells, respectively, compared to those of the BMDCs incubated with the untreated group.

Cancer Cells Treated with Au-DOX@PO-ANG are Effective Vaccines in vivo

A well-established in vivo mouse G422 cancer vaccination experiment was carried out in immunocompetent C57BL/6 J mice to investigate the ability of treated cancer cells to activate the adaptive immune system.[36] C57BL/6J mice were immunized with G422 cells that died after Au-DOX@PO-ANG+RT treatment. Negative control mice were injected with PBS. The mice were then challenged with live G422 tumour cells. Changes in tumour volume at the challenge site were observed using MRI (Figure 6A). Tumour growth was observed in the mice immunized with PBS. Mice immunized with G422 cells treated with RT, Au-DOX@PO-ANG, or Au-DOX@PO-ANG+RT showed signs of protection against tumour growth. Among them, mice immunized with G422 cells treated with Au-DOX@PO-ANG+RT showed the most obvious inhibition of tumour growth. Furthermore, the tumours growing in the PBS-vaccinated mice at the challenge site were large in size and occurred earlier (Figure 6B), indicating that induction of death in cancer cells by Au-DOX@PO-ANG+RT activates an adaptive immune response. It is one of the important properties of ICD. Finally, we note a potential limitation of this study: these ideal in vivo data are related to the inevitable destruction of the blood–brain barrier when constructing orthotopic xenograft tumour models, making it more susceptible to immunotherapy.

IFN-γ, TNF-α, and IL-12/p40 Level in Mouse Serum

We used ELISA kits to detect IFN-γ, TNF-α, and IL-12/p40 levels in the serum of mice in each treatment group. The result is shown in Figure 7. In this study, the normal group refers to healthy mice that have not been challenged by live cells. Au-DOX@PO-ANG+RT group of IFN-γ Level is 2971.9±307.3 pg/mL, significantly higher than PBS group (63.4±53.2 pg/mL), RT group (1775.1±220.2 pg/mL), and Au-DOX@PO-ANG group (2275.0±316.1 pg/mL)(Figure 7A). In addition, the levels of the innate/adaptive immunity regulator interleukin 12 (IL-12p40) and tumour necrosis factor α (TNF-α) in serum were also

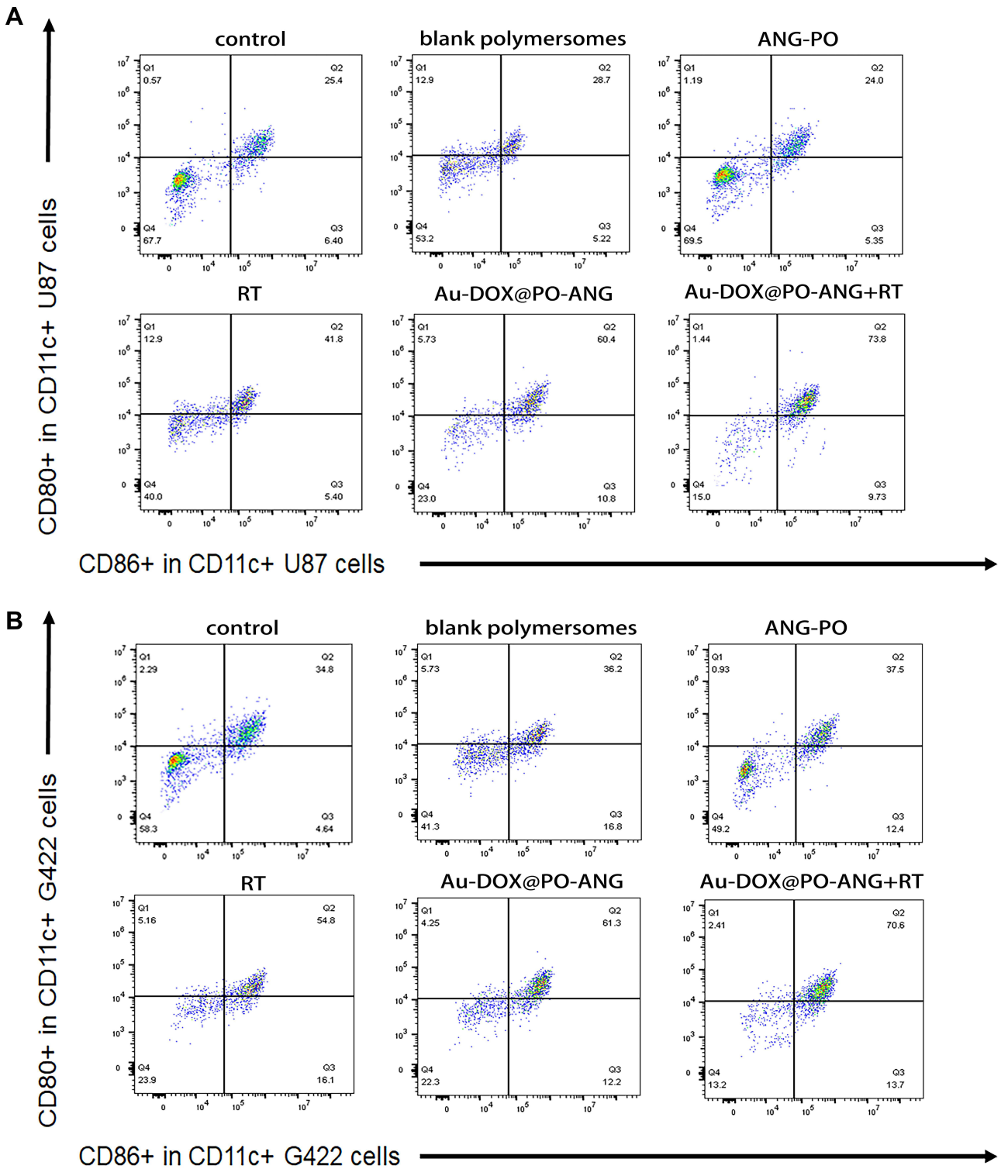

Figure 5 The analysis of BMDCs maturation in vitro. Representative flow cytometry and quantitative analysis of mature BMDC cells (CD80+/CD86+in CD11c+). Co-culture of BMDCs with dying U87-MG (**A**)and G422 (**B**) cells.

measured. As demonstrated in Figure 7B and C. Au-DOX@PO-ANG combined with RT led to an enhanced immune response (both cytokine levels were significantly improved compared with the PBS group). These results demonstrate the powerful immunoprotective effect induced by Au-DOX@PO-ANG combined with RT.

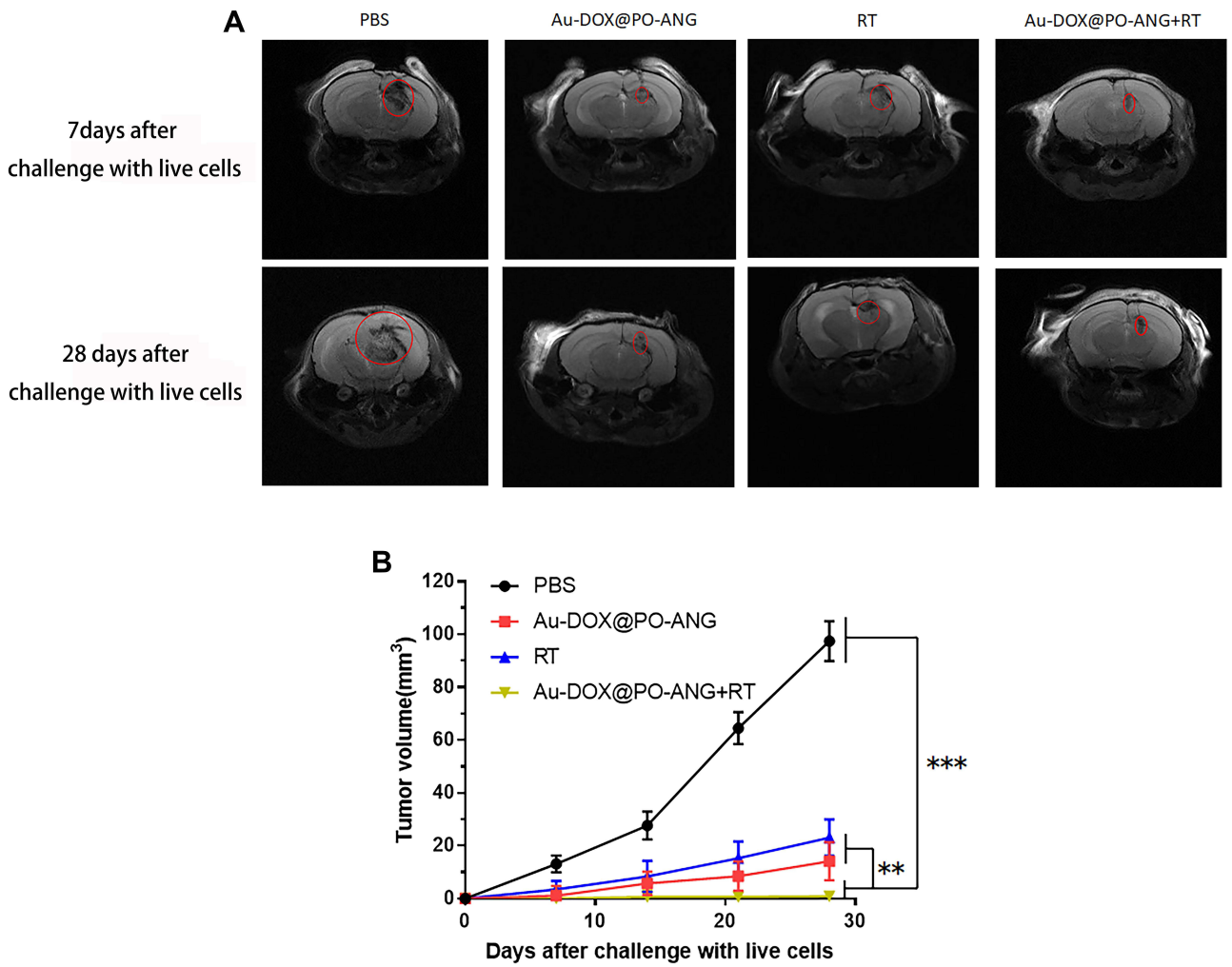

Figure 6 Tumor cells dying after different treatments induce anti-tumor immunogenicity in vivo. (**A**) MIR images of each group 7 days and 28 days after challenge with live cells, the regions in the red circles are the glioblastoma area; (**B**) The size of the tumors growing at the challenge site of the mice in the prophylactic tumor vaccination experiments used in (**A**). Each bar represents the mean± SD of six replicates, **P<0.01,***P<0.001.

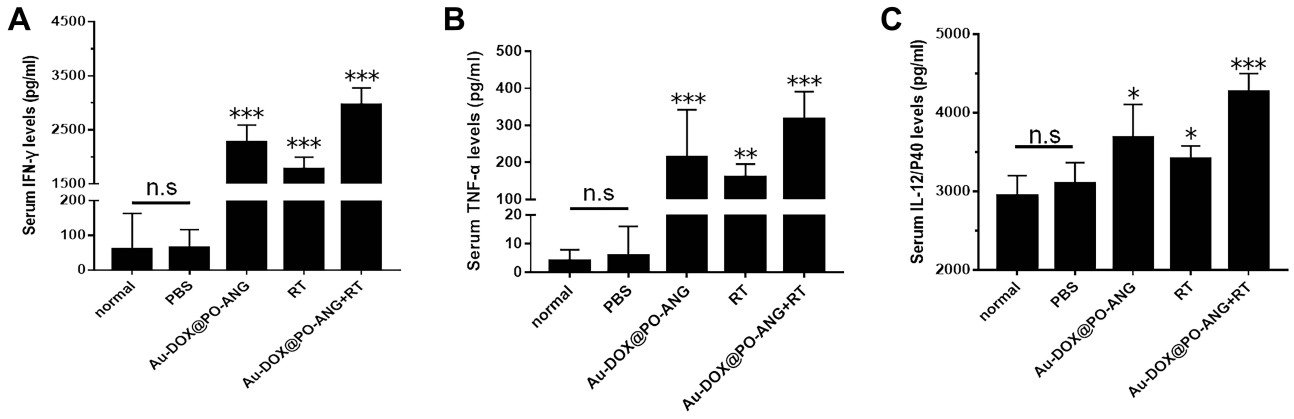

Figure 7 Vaccinated with different tumor vaccines, cytokine levels in serum of mice isolated 7 days after challenged with live cells. IFN-γ (**A**), TNF-α (**B**) and IL-12/p40 (**C**) level in mouse serum. Each bar represents the mean± SD of six replicates, *P<0.05, **P<0.01,***P<0.001.

Discussion

ICD is a method of cell death that can induce the immune response to tumour cells. Calreticulin (CRT), HMGB1, ATP, and other damage-associated molecular patterns (DAMPs) are released when immunogenic cell death occurs.[10,37,38] Previously, a new type of pH-sensitive cargo-loaded polymersomes was designed. There are many studies indicate that tumor tissue has special physiological characteristics. The pH value of the tumor microenvironment is 6.5–7.0, which is lower than that of normal tissues (pH 7.4). The pH-sensitive nano-drug delivery system of the tumor's acidic environment can increase the drug delivery in tumor tissues.[39] The pH-responsive strategies can increase the functionality of drug delivery system.[40–42] The pH sensitivity of the drug has been evaluated in previous studies.[32] In this study, we evaluated the ability of the previously constructed pH-sensitive nanodrug delivery system to induce immunogenic cell death in tumour cells. Due to the particularity of the immune microenvironment in the brain,[43] there are few studies on the immunotherapy of brain tumours, and this study is a bold attempt at immune-related treatments for brain tumours. We prove that the new pH-sensitive nanodrug delivery system can activate the antitumour immune response by inducing immunogenic cell death of tumour cells and provide new strategies and directions for brain tumour immunotherapy.

First, to evaluate the ICD effect, the effect of Au-DOX@PO-ANG combined with RT induced in cancer cells was evaluated, and the drug concentration was controlled at approximately the IC50. The confocal laser confocal microscopy images show that CRT will evert to the cell membrane when ICD occurs. CRT mainly exists in the endoplasmic reticulum, and the eversion of CRT is related to Au-DOX@PO-ANG combined with RT, which can induce endoplasmic reticulum stress.[16,44,45] At the same time, we proved that Au-DOX@PO-ANG combined with RT could induce the emission of HMGB1 and ATP. Of course, only Au-DOX@PO-ANG or radiotherapy can also cause the release of DAMPs. Doxorubicin is a chemotherapeutic that has been shown to induce ICD.[25,26] Radiotherapy is also a treatment that can induce ICD in tumour cells, and the presence of radiotherapy sensitizer AuNPs may enhance this effect.[46] However, the combination of the two can induce stronger ICD effects in tumour cells and induce the activation and maturation of BMDCs. Tumour vaccine experiment results have shown that the injection of dying necroptotic cancer cells directly leads to more effective control of tumour growth in mice. However, there is a potential limitation of this study: these ideal in vivo data are related to the inevitable destruction of the blood–brain barrier when constructing orthotopic xenograft tumour models, making them more susceptible to immunotherapy. In the future, our work will focus on improving experimental methods to provide more directions for immune-related treatment of glioblastoma.

Conclusion

Dying cancer cells induced by Au-DOX@PO-ANG+RT could induce calreticulin eversion to the cell membrane, promote the release of HMGB1 and ATP, and induce the maturation of BMDCs. Using dying cancer cells induced by Au-DOX@PO-ANG+RT, we demonstrate the efficient vaccination potential of ICD in vivo. These results identify Au-DOX@PO-ANG as a novel immunogenic cell death inducer in vitro and in vivo that can be effectively combined with RT in cancer therapy.

Data Sharing Statement

The datasets used and analysed during the current study are available from the corresponding author on reasonable request.

Ethics Approval and Consent to Participate

All animal procedures were performed according to the Institutional Animal Care & Use Committee at Southeast University and the committee approved this study. The ethical number was 20170131016.

Author Contributions

QT and ZZ contributed to the design and conception of the subject; CH was responsible for the implementation of the experiments and paper writing; HD and JC performed the animal imaging; YD and RY contributed to data analysis; YA and CH gave lots of guidance on experiment details and paper submission. DL and PL were helpful in animal model construction and picture processing. All authors made substantial contributions to conception and design, acquisition of data, or analysis and interpretation of data; took part in drafting the article or revising it critically for important intellectual content; agreed to submit to the current journal; gave final approval of the version to be published; and agree to be accountable for all aspects of the work.

Funding

This work was supported by the high-level talents (333 Project) of Jiangsu Province (BRA2019024); the National Natural Science Foundation of China (81602728); the National Natural Science Foundation of China (81571789); the National Natural Science Foundation of China (81771980); the Key Project Foundation of Jiangsu Health and Health Committee (H2018114); the Social Development Project of the Key Research and Development Plan of Jiangsu Province (BE2018606); the China Postdoctoral Science Foundation Funded Project (2018M630605); the Youth Talent's Project of Jiangsu Province (QNRC2016164) and the Provincial Foundation of Jiangsu Province (20171148).

Disclosure

The authors have declared that no competing interests exist.

References

1. Tanaka S, Louis DN, Curry WT, Batchelor TT, Dietrich J. Diagnostic and therapeutic avenues for glioblastoma: no longer a dead end? *Nat Rev Clin Oncol*. 2013;10(1):14–26. doi:10.1038/nrclinonc.2012.204
2. Orive G, Ali OA, Anitua E, Pedraz JL, Emerich DF. Biomaterial-based technologies for brain anti-cancer therapeutics and imaging. *Biochim Biophys Acta*. 2010;1806(1):96–107.
3. Lapointe S, Perry A, Butowski NA. Primary brain tumours in adults. *Lancet*. 2018;392(10145):432–446. doi:10.1016/S0140-6736(18)30990-5
4. Alphandery E. Nano-therapies for glioblastoma treatment. *Cancers*. 2020;12(1):242. doi:10.3390/cancers12010242
5. Alphandery E, Idbaih A, Adam C, et al. Biodegraded magnetosomes with reduced size and heating power maintain a persistent activity against intracranial U87-Luc mouse GBM tumors. *J Nanobiotechnology*. 2019;17(1):126. doi:10.1186/s12951-019-0555-2
6. Alphandery E. Glioblastoma treatments: an account of recent industrial developments. *Front Pharmacol*. 2018;9:879. doi:10.3389/fphar.2018.00879
7. Hamdous Y, Chebbi I, Mandawala C, et al. Biocompatible coated magnetosome minerals with various organization and cellular interaction properties induce cytotoxicity towards RG-2 and GL-261 glioma cells in the presence of an alternating magnetic field. *J Nanobiotechnology*. 2017;15(1):74. doi:10.1186/s12951-017-0293-2
8. Byun DJ, Wolchok JD, Rosenberg LM, Girotra M. Cancer immunotherapy - immune checkpoint blockade and associated endocrinopathies. *Nat Rev Endocrinol*. 2017;13(4):195–207. doi:10.1038/nrendo.2016.205
9. Stewart TJ, Abrams SI. How tumours escape mass destruction. *Oncogene*. 2008;27(45):5894–5903. doi:10.1038/onc.2008.268
10. Casares N, Pequignot MO, Tesniere A, et al. Caspase-dependent immunogenicity of doxorubicin-induced tumor cell death. *J Exp Med*. 2005;202(12):1691–1701. doi:10.1084/jem.20050915
11. Galluzzi L, Buque A, Kepp O, Zitvogel L, Kroemer G. Immunogenic cell death in cancer and infectious disease. *Nat Rev Immunol*. 2017;17(2):97–111. doi:10.1038/nri.2016.107
12. Apetoh L, Ghiringhelli F, Tesniere A, et al. Toll-like receptor 4-dependent contribution of the immune system to anticancer chemotherapy and radiotherapy. *Nat Med*. 2007;13(9):1050–1059. doi:10.1038/nm1622
13. Garg AD, Krysko DV, Vandenabeele P, Agostinis P. Extracellular ATP and P(2)X(7) receptor exert context-specific immunogenic effects after immunogenic cancer cell death. *Cell Death Dis*. 2016;7:e2097. doi:10.1038/cddis.2015.411
14. Garg AD, Krysko DV, Vandenabeele P, Agostinis P. Hypericin-based photodynamic therapy induces surface exposure of damage-associated molecular patterns like HSP70 and calreticulin. *Cancer Immunol Immunother*. 2012;61(2):215–221. doi:10.1007/s00262-011-1184-2
15. Kroemer G, Galluzzi L, Kepp O, Zitvogel L. Immunogenic cell death in cancer therapy. *Annu Rev Immunol*. 2013;31:51–72. doi:10.1146/annurev-immunol-032712-100008
16. Krysko DV, Garg AD, Kaczmarek A, Krysko O, Agostinis P, Vandenabeele P. Immunogenic cell death and DAMPs in cancer therapy. *Nat Rev Cancer*. 2012;12(12):860–875. doi:10.1038/nrc3380
17. Tesniere A, Schlemmer F, Boige V, et al. Immunogenic death of colon cancer cells treated with oxaliplatin. *Oncogene*. 2010;29(4):482–491. doi:10.1038/onc.2009.356
18. Formenti SC, Demaria S. Systemic effects of local radiotherapy. *Lancet Oncol*. 2009;10(7):718–726. doi:10.1016/S1470-2045(09)70082-8
19. Rodriguez-Ruiz ME, Vanpouille-Box C, Melero I, Formenti SC, Demaria S. Immunological mechanisms responsible for radiation-induced abscopal effect. *Trends Immunol*. 2018;39(8):644–655. doi:10.1016/j.it.2018.06.001
20. Xie J, Gong L, Zhu S, Yong Y, Gu Z, Zhao Y. Emerging strategies of nanomaterial-mediated tumor radiosensitization. *Adv Mater*. 2019;31(3):e1802244. doi:10.1002/adma.201802244
21. Chithrani DB, Jelveh S, Jalali F, et al. Gold nanoparticles as radiation sensitizers in cancer therapy. *Radiat Res*. 2010;173(6):719–728. doi:10.1667/RR1984.1
22. Her S, Jaffray DA, Allen C. Gold nanoparticles for applications in cancer radiotherapy: mechanisms and recent advancements. *Adv Drug Deliv Rev*. 2017;109:84–101. doi:10.1016/j.addr.2015.12.012
23. Daraee H, Eatemadi A, Abbasi E, Fekri Aval S, Kouhi M, Akbarzadeh A. Application of gold nanoparticles in biomedical and drug delivery. *Artif Cells Nanomed Biotechnol*. 2016;44(1):410–422. doi:10.3109/21691401.2014.955107
24. Hainfeld JF, Dilmanian FA, Zhong Z, Slatkin DN, Kalef-Ezra JA, Smilowitz HM. Gold nanoparticles enhance the radiation therapy of a murine squamous cell carcinoma. *Phys Med Biol*. 2010;55(11):3045–3059. doi:10.1088/0031-9155/55/11/004
25. Amaravadi RK, Thompson CB. The roles of therapy-induced autophagy and necrosis in cancer treatment. *Clin Cancer Res*. 2007;13(24):7271–7279. doi:10.1158/1078-0432.CCR-07-1595
26. Kepp O, Tesniere A, Zitvogel L, Kroemer G. The immunogenicity of tumor cell death. *Curr Opin Oncol*. 2009;21(1):71–76. doi:10.1097/CCO.0b013e32831bc375
27. He C, Tang Z, Tian H, Chen X. Co-delivery of chemotherapeutics and proteins for synergistic therapy. *Adv Drug Deliv Rev*. 2016;98:64–76. doi:10.1016/j.addr.2015.10.021
28. He C, Duan X, Guo N, et al. Core-shell nanoscale coordination polymers combine chemotherapy and photodynamic therapy to potentiate checkpoint blockade cancer immunotherapy. *Nat Commun*. 2016;7:12499. doi:10.1038/ncomms12499
29. Obeid M, Tesniere A, Ghiringhelli F, et al. Calreticulin exposure dictates the immunogenicity of cancer cell death. *Nat Med*. 2007;13(1):54–61. doi:10.1038/nm1523
30. Lu YC, Weng WC, Lee H. Functional roles of calreticulin in cancer biology. *Biomed Res Int*. 2015;2015:526524. doi:10.1155/2015/526524
31. Gardai SJ, McPhillips KA, Frasch SC, et al. Cell-surface calreticulin initiates clearance of viable or apoptotic cells through trans-activation of LRP on the phagocyte. *Cell*. 2005;123(2):321–334. doi:10.1016/j.cell.2005.08.032

32. He C, Zhang Z, Ding Y, et al. LRP1-mediated pH-sensitive polymersomes facilitate combination therapy of glioblastoma in vitro and in vivo. *J Nanobiotechnology*. 2021;19(1):29. doi:10.1186/s12951-020-00751-x
33. Hainfeld JF, Slatkin DN, Smilowitz HM. The use of gold nanoparticles to enhance radiotherapy in mice. *Phys Med Biol*. 2004;49(18):N309–N3015. doi:10.1088/0031-9155/49/18/N03
34. Dong X, Cheng R, Zhu S, et al. A heterojunction structured WO2.9-WSe2 nanoradiosensitizer increases local tumor ablation and checkpoint blockade immunotherapy upon low radiation dose. *ACS Nano*. 2020;14(5):5400–5416. doi:10.1021/acsnano.9b08962
35. Yamazaki T, Hannani D, Poirier-Colame V, et al. Defective immunogenic cell death of HMGB1-deficient tumors: compensatory therapy with TLR4 agonists. *Cell Death Differ*. 2014;21(1):69–78. doi:10.1038/cdd.2013.72
36. Sukkurwala AQ, Adjemian S, Senovilla L, et al. Screening of novel immunogenic cell death inducers within the NCI mechanistic diversity set. *Oncoimmunology*. 2014;3(4):e28473. doi:10.4161/onci.28473
37. Zhou J, Wang G, Chen Y, Wang H, Hua Y, Cai Z. Immunogenic cell death in cancer therapy: present and emerging inducers. *J Cell Mol Med*. 2019;23(8):4854–4865. doi:10.1111/jcmm.14356
38. Pitt JM, Kroemer G, Zitvogel L. Immunogenic and non-immunogenic cell death in the tumor microenvironment. *Adv Exp Med Biol*. 2017;1036:65–79.
39. Kanamala M, Wilson WR, Yang M, Palmer BD, Wu Z. Mechanisms and biomaterials in pH-responsive tumour targeted drug delivery: a review. *Biomaterials*. 2016;85:152–167. doi:10.1016/j.biomaterials.2016.01.061
40. Li J, Anraku Y, Kataoka K. Self-boosting catalytic nanoreactors integrated with triggerable crosslinking membrane networks for initiation of immunogenic cell death by pyroptosis. *Angew Chem Int Ed Engl*. 2020;59(32):13526–13530. doi:10.1002/anie.202004180
41. Alphandery E, Abi Haidar D, Seksek O, et al. Nanoprobe synthesized by magnetotactic bacteria, detecting fluorescence variations under dissociation of rhodamine B from magnetosomes following temperature, pH changes, or the application of radiation. *ACS Appl Mater Interfaces*. 2017;9(42):36561–36572. doi:10.1021/acsami.7b09720
42. Mandawala C, Chebbi I, Durand-Dubief M, et al. Biocompatible and stable magnetosome minerals coated with poly-l-lysine, citric acid, oleic acid, and carboxy-methyl-dextran for application in the magnetic hyperthermia treatment of tumors. *J Mater Chem B*. 2017;5(36):7644–7660. doi:10.1039/C6TB03248F
43. Du B, Waxman DJ. Medium dose intermittent cyclophosphamide induces immunogenic cell death and cancer cell autonomous type I interferon production in glioma models. *Cancer Lett*. 2020;470:170–180. doi:10.1016/j.canlet.2019.11.025
44. Garg AD, Krysko DV, Vandenabeele P, Agostinis P. The emergence of phox-ER stress induced immunogenic apoptosis. *Oncoimmunology*. 2012;1(5):786–788. doi:10.4161/onci.19750
45. Panaretakis T, Kepp O, Brockmeier U, et al. Mechanisms of pre-apoptotic calreticulin exposure in immunogenic cell death. *EMBO J*. 2009;28(5):578–590. doi:10.1038/emboj.2009.1
46. Janic B, Brown SL, Neff R, et al. Therapeutic enhancement of radiation and immunomodulation by gold nanoparticles in triple negative breast cancer. *Cancer Biol Ther*. 2021;22(2):124–135. doi:10.1080/15384047.2020.1861923